



## Perspectives on Proterozoic surface ocean redox from iodine contents in ancient and recent carbonate



Dalton S. Hardisty<sup>a,l,\*</sup>, Zunli Lu<sup>b</sup>, Andrey Bekker<sup>a,c</sup>, Charles W. Diamond<sup>a</sup>, Benjamin C. Gill<sup>d</sup>, Ganqing Jiang<sup>e</sup>, Linda C. Kah<sup>f</sup>, Andrew H. Knoll<sup>g</sup>, Sean J. Loyd<sup>h</sup>, Magdalena R. Osburn<sup>i</sup>, Noah J. Planavsky<sup>j</sup>, Chunjiang Wang<sup>k</sup>, Xiaoli Zhou<sup>b</sup>, Timothy W. Lyons<sup>a</sup>

<sup>a</sup> Department of Earth Sciences, University of California, Riverside, CA, USA

<sup>b</sup> Department of Earth Sciences, Syracuse University, Syracuse, NY, USA

<sup>c</sup> Department of Geology, University of Johannesburg, South Africa

<sup>d</sup> Department of Geosciences, Virginia Polytechnic and State University, Blacksburg, VA, USA

<sup>e</sup> Department of Geoscience, University of Nevada, Las Vegas, NV, USA

<sup>f</sup> Department of Earth and Planetary Sciences, University of Tennessee, Knoxville, TN, USA

<sup>g</sup> Department of Earth and Planetary Sciences, Harvard University, Cambridge, MA, USA

<sup>h</sup> Department of Geological Sciences, California State University, Fullerton, CA, USA

<sup>i</sup> Department of Earth and Planetary Sciences, Northwestern University, Evanston, IL, USA

<sup>j</sup> Department of Geology and Geophysics, Yale University, New Haven, CT, USA

<sup>k</sup> College of Geosciences, China University of Petroleum, Beijing, China

<sup>l</sup> Department of Geology and Geophysics, Woods Hole Oceanographic Institute, Woods Hole, MA, USA

### ARTICLE INFO

#### Article history:

Received 10 September 2016

Received in revised form 23 January 2017

Accepted 25 January 2017

Available online 14 February 2017

Editor: H. Stoll

#### Keywords:

Proterozoic oxygen  
Shuram isotope anomaly  
carbonate diagenesis  
Bahamas  
iodine  
metazoan evolution

### ABSTRACT

The Proterozoic Eon hosted the emergence and initial recorded diversification of eukaryotes. Oxygen levels in the shallow marine settings critical to these events were lower than today's, although how much lower is debated. Here, we use concentrations of iodate (the oxidized iodine species) in shallow-marine limestones and dolostones to generate the first comprehensive record of Proterozoic near-surface marine redox conditions. The iodine proxy is sensitive to both local oxygen availability and the relative proximity to anoxic waters. To assess the validity of our approach, Neogene–Quaternary carbonates are used to demonstrate that diagenesis most often decreases and is unlikely to increase carbonate-iodine contents. Despite the potential for diagenetic loss, maximum Proterozoic carbonate iodine levels are elevated relative to those of the Archean, particularly during the Lomagundi and Shuram carbon isotope excursions of the Paleo- and Neoproterozoic, respectively. For the Shuram anomaly, comparisons to Neogene–Quaternary carbonates suggest that diagenesis is not responsible for the observed iodine trends. The baseline low iodine levels in Proterozoic carbonates, relative to the Phanerozoic, are linked to a shallow oxic–anoxic interface. Oxygen concentrations in surface waters would have at least intermittently been above the threshold required to support eukaryotes. However, the diagnostically low iodine data from mid-Proterozoic shallow-water carbonates, relative to those of the bracketing time intervals, are consistent with a dynamic chemocline and anoxic waters that would have episodically mixed upward and laterally into the shallow oceans. This redox instability may have challenged early eukaryotic diversification and expansion, creating an evolutionary landscape unfavorable for the emergence of animals.

© 2017 Elsevier B.V. All rights reserved.

### 1. Introduction

The shallow oceans of the Proterozoic Eon were the host to both photosynthetic oxygen production and the sequential origin

\* Corresponding author at: Department of Geology and Geophysics, Woods Hole Oceanographic Institute, Woods Hole, MA, USA.

E-mail address: dhardisty@whoi.edu (D.S. Hardisty).

and radiations of eukaryotes and animals (Knoll, 2014; Lyons et al., 2014). Nevertheless, the current conversation about the oxygenation of the biosphere, the first appearances and diversification of the earliest eukaryotes and animals, and their associated oxygen demands (Mills et al., 2014; Sperling et al., 2013) has often focused instead on conditions in the atmosphere (Planavsky et al., 2014) and sub-photic deep-marine waters (Gilleaudeau and Kah, 2015;

Partin et al., 2013; Reinhard et al., 2013; Sperling et al., 2015). Such comparisons are indirect, since *in situ* oxygenic photosynthesis in the shallow photic zone provides the potential for elevated shallow-ocean oxygen at micromolar ( $\mu\text{M}$ ) levels even under an anoxic atmosphere (Reinhard et al., 2016). This disconnect reflects a shortage of carbonate geochemical redox proxies specific to local shallow ocean conditions. The need to fill this knowledge gap is particularly critical through the mid-Proterozoic (ca. 1.8 to 0.8 billion years ago or Ga), which precedes the evolution of the earliest metazoans (Knoll, 2014).

Geochemical proxies that track the mobilization of iron and manganese in mid-Proterozoic soils are consistent with mid-Proterozoic  $p\text{O}_2$  as low as  $<0.1\text{--}1\%$  of present atmospheric levels (PAL) (Cole et al., 2016; Crowe et al., 2013; Mitchell and Sheldon, 2009; Planavsky et al., 2014). If these estimates are correct, the predicted nanomolar (nM) to low  $\mu\text{M}$  equilibrium-driven levels of dissolved  $\text{O}_2$  in the surface ocean are likely to have inhibited eukaryote diversification (Planavsky et al., 2014; Reinhard et al., 2016). Limited carbonate paleoredox proxy records (REE's, Zn/Fe) are generally consistent with low atmospheric  $p\text{O}_2$  through portions of the Proterozoic (Liu et al., 2016; Tang et al., 2016) and extensive records of redox-sensitive metals (Mo, Cr, U, Fe) in basinal black shale specifically fingerprint an anoxic deeper ocean dominated by a combination of ferruginous and sulfidic (euxinic) waters (Gilleaudeau and Kah, 2015; Partin et al., 2013; Reinhard et al., 2013; Sperling et al., 2015).

Ratios of iodine-to-calcium-magnesium, or  $I/(\text{Ca} + \text{Mg})$ , in shallow-marine carbonates can track the presence or absence of  $\text{O}_2$  in the shallow ocean (Hardisty et al., 2014) and the position of the oxic–anoxic interface in the water column relative to the site of carbonate precipitation (Lu et al., 2016). The oxidized and reduced iodine species, iodate ( $\text{IO}_3^-$ ) and iodide ( $\text{I}^-$ ), respectively, constitute the bulk of total dissolved iodine ( $\text{IO}_3^- + \text{I}^-$ ) in seawater (Chance et al., 2014; Emerson et al., 1979; Farrenkopf and Luther III, 2002; Rue et al., 1997; Wong and Brewer, 1977). In marine waters,  $\text{IO}_3^-$  and  $\text{I}^-$  concentrations are inversely correlated, with nearly uniform vertical profiles of total dissolved iodine outside of a slight depletion in photic waters. Concentrations of total dissolved iodine in modern seawater are near 450–500 nM (Chance et al., 2014), globally uniform, and have a residence time ( $\sim 300$  kyrs) that is orders of magnitude longer than the mixing time of the ocean. Importantly,  $\text{IO}_3^-$  exists exclusively in oxic waters, with  $\text{IO}_3^-$  reduction occurring in weakly oxic waters prior to the onset of iron and sulfate reduction (Fig. 1; Emerson et al., 1979; Farrenkopf and Luther III, 2002; Kennedy and Elderfield, 1987a, 1987b; Rue et al., 1997; Wong and Brewer, 1977). Quantitative  $\text{IO}_3^-$  reduction is observed within anoxic basins (Emerson et al., 1979; Wong and Brewer, 1977) and in reducing pore waters (Kennedy and Elderfield, 1987a, 1987b). The redox behavior of iodine can be traced for ancient oceans because  $\text{IO}_3^-$  is the sole iodine species that co-precipitates with carbonate rocks (Lu et al., 2010). Thus, carbonate minerals formed in anoxic waters—where  $\text{I}^-$  is the predominant dissolved iodine species—are not expected to incorporate iodine during precipitation, as demonstrated in calcite synthesis experiments (Lu et al., 2010). This expectation is consistent with previous reports noting a lack of iodine in carbonate rocks prior to the Great Oxidation Event (GOE) (Hardisty et al., 2014).

Although quantitative reduction of  $\text{IO}_3^-$  occurs within hours in low-oxygen and anoxic waters (Farrenkopf et al., 1997),  $\text{I}^-$  oxidation can be a slower process, with rate estimates ranging from weeks to years (Chance et al., 2014; Luther III et al., 1995). Due to this redox asymmetry, the largest gradients in marine  $\text{IO}_3^-$  concentrations occur within the oxycline of oxygen-minimum zone (OMZs) or anoxic basins (Fig. 1; Farrenkopf and Luther III, 2002; Rue et al., 1997). In this weakly oxic zone,  $\text{IO}_3^-$  reduction becomes favorable but is not quantitative and together with both *in*

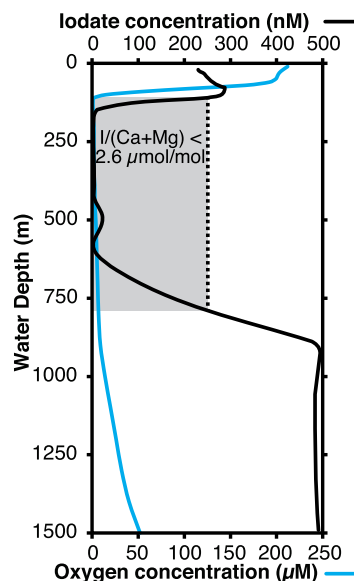


Fig. 1. Water column dissolved  $[\text{IO}_3^-]$  and  $[\text{O}_2]$  from a vertical transect through the Peruvian OMZ (Rue et al., 1997). The vertical dashed line highlights the range of  $[\text{IO}_3^-]$  ( $<250$  nM) that is nearly exclusively observed in settings within or below the oxycline of marine anoxic basins and OMZs (Lu et al., 2016). The shaded box refers to the portion of the profile where corresponding  $I/(\text{Ca} + \text{Mg})$  ratios are anticipated to be  $<2.6$   $\mu\text{mol/mol}$  (Glock et al., 2014; Lu et al., 2016), which is further discussed in the main text.

*situ* production and *ex situ* input of the relatively slow oxidizing  $\text{I}^-$ —transported from underlying anoxic waters characterized by quantitative  $\text{IO}_3^-$  reduction—results in steep  $[\text{IO}_3^-]$  gradients (Farrenkopf and Luther III, 2002; Lu et al., 2016; Rue et al., 1997; Wong and Brewer, 1977). Modern seawater non-zero  $[\text{IO}_3^-]$  values of  $<250$  nM are almost exclusively found in such settings (Fig. 1; Chance et al., 2014; Lu et al., 2016). This low range of seawater  $[\text{IO}_3^-]$  would be recorded as  $I/(\text{Ca} + \text{Mg})$  ratios of  $<\sim 2.6$   $\mu\text{mol/mol}$  in carbonate, as observed in both laboratory calcite-precipitation experiments (Lu et al., 2010) and direct measurements of modern carbonate from low oxygen settings (Glock et al., 2014; Lu et al., 2016). Analogous to the oxyclines of modern OMZs and anoxic basins, ancient carbonate with non-zero  $I/(\text{Ca} + \text{Mg})$  of less than  $\sim 2.6$   $\mu\text{mol/mol}$  are interpreted to reflect precipitation within waters with local  $\text{O}_2$  levels above those necessary to sustain  $\text{IO}_3^-$  accumulation, but which are also characterized by or in frequent exchange with waters hosting active  $\text{IO}_3^-$  reduction (Lu et al., 2016).

Importantly, diagenetic effects on  $I/(\text{Ca} + \text{Mg})$  ratios have not been examined in previous studies. Given that diagenetic carbonate minerals form most often from anoxic pore fluids (Lloyd et al., 2012; McClain et al., 1992; Schrag et al., 2013) marked by  $\text{IO}_3^-$  reduction, carbonate phases are expected to be particularly sensitive to diagenetic iodine loss. Carbonates of the Proterozoic Eon host the largest positive and negative  $\delta^{13}\text{C}_{\text{carb}}$  excursions in Earth history—the Paleoproterozoic Lomagundi and Ediacaran Shuram anomalies, respectively. Although differing in direction, both have been interpreted as large-scale Proterozoic oxidation events bracketing the overall mid-Proterozoic low oxygen atmosphere (e.g., Fike et al., 2006; Lyons et al., 2014). However, these records are at best only indirect measures of redox conditions in the surface ocean, and their relationships to the broader workings of the carbon cycle as manifested in marine water column signals can be lost or overprinted during diagenesis by pore fluid chemistry (Schrag et al., 2013; Swart and Kennedy, 2012). If the effects of diagenesis on  $I/(\text{Ca} + \text{Mg})$  are understood, examination of  $I/(\text{Ca} + \text{Mg})$  through Proterozoic carbon isotope excursions may provide a means of testing whether these records represent pore fluid or water column chemistry.

**Table 1**

Approximate ages and number of samples for Proterozoic geologic units measured for I/(Ca+Mg) ratios in this study. References to ages and lithological descriptions can be found in the supplementary materials.

Geologic unit	Approximate age (billions of years)	<i>n</i>
Woolly Dolomite, Australia	2.03	11
Snare Group, Canada	1.97	4
Taltheilei Formation, Canada	1.88	14
Duck Creek Formation, Australia	1.80	22
Paradise Creek Formation, Australia	1.65	10
Helena Formation, USA	1.45	9
Tieling Formation, China	1.44	45
Kaltasy Formation, Russia	1.43	12
Dismal Lakes Group, Canada	1.30	16
Mescal Formation, USA	1.26	4
Angmaat Formation, Canada	1.15	17
Atar and El Mreiti groups, Mauritania	1.10	17
Sukhaya Tunguska Formation, Russia	1.04	7
Shaler Group, Canada	0.85	17
Akademikerbeen Group, Svalbard; Limestone-Dolomite Series, Greenland	0.83	36
Beck Springs Dolomite, USA	0.75	20
Khufai Formation, Sultanate of Oman	0.58	122
Johnnie Formation, USA	0.58	30
Clemente Formation, Mexico	0.58	31
Doushantuo Formation, China (Siduping)	0.64–0.58	74

Here we provide the most comprehensive record of Proterozoic surface ocean redox to date, specifically tracking temporal marine  $\text{IO}_3^-$  availability through a compilation of I/(Ca+Mg) ratios from mostly shallow-marine carbonate rocks (limestones and dolostones). This data set includes carbonates capturing the Shuram  $\delta^{13}\text{C}_{\text{carb}}$  excursion. We also provide the first constraints on iodine proxy response to diagenetic alteration of recent carbonates. Through comparisons of dissolved iodine cycling in modern low-oxygen versus well-oxygenated marine waters, I/(Ca+Mg) records from pristine modern carbonates from both redox end members, and diagenetic carbonates from Neogene–Quaternary settings, we suggest that oxygenation in the surface ocean following the GOE was consistent with that necessary to sustain simple eukaryotic life. At the same time, the low I/(Ca+Mg) ratios typical of the mid-Proterozoic reflect carbonate precipitation in waters with overall low and unstable oxygen levels in close spatial proximity to anoxic waters. In addition, we provide evidence against diagenesis as a driver of the Shuram excursion.

## 2. Materials

We measured I/(Ca+Mg) ratios of carbonate rocks ( $n = 518$ ) from 20 sedimentary successions spanning the late Paleoproterozoic to late Neoproterozoic (Table 1) and combined these results with previously published carbonate iodine data (Glock et al., 2014; Hardisty et al., 2014; Loope et al., 2013; Lu et al., 2016, 2010; Owens et al., 2017; Zhou et al., 2014, 2015). Details regarding age, stratigraphy, and complementary geochemistry for the individual sections are included in the Supplementary Materials. This data set also includes new results from four previously studied carbonate sections that capture the Ediacaran Shuram negative  $\delta^{13}\text{C}_{\text{carb}}$  anomaly: the Khufai Formation of the Sultanate of Oman (Osburn et al., 2015); the Doushantuo Formation of South China; the Johnnie Formation of Death Valley, USA; and the Clemente Formation of northern Mexico (Loyd et al., 2013). For this and the previously published Precambrian iodine data (Hardisty et al., 2014), emphasis was placed on carbonate successions with independent sedimentological evidence for shallow-marine deposition and units with clear indications of secondary alteration, such as veins and metamorphism above greenschist grade, were avoided.

**Table 2**

Approximate ages and number of samples for Neogene–Quaternary geologic units measured for I/(Ca+Mg) ratios in this study. Also shown are the diagenetic conditions affecting mineralogy at each study site. The relevant previous publications providing lithological, geochemical, and diagenetic constraints are provided in the Supplementary Materials and in some cases in the main text. Supplementary Fig. 1 contains a map of the sampling localities.

Age	Location	Diagenetic setting	<i>n</i>
Modern	Little Darby and Lee Stocking Islands, Bahamas	initial deposition	57
Pleistocene	Key Largo Limestone, South Florida	initial deposition, meteoric	30
Neogene–Quaternary	Clino, Bahamas	meteoric, marine burial, dolomitization	151
Neogene–Quaternary	Unda, Bahamas	dolomitization	49
Miocene	Monterey Formation, Central California	authigenic dolomite concretions	24

To evaluate the effects of diagenetic mineral transformations on I/(Ca+Mg) ratios, we include a series of Neogene–Quaternary case studies to provide a comprehensive view of initial iodine precipitation and subsequent modification as a function of varying primary carbonate mineralogy, carbonate burial history, and related diagenetic pathways—specifically, meteoric diagenesis, marine burial diagenesis, and dolomitization. The case studies are outlined below (along with citations to detailed previous studies of the same localities or samples), in Table 2, and in the Supplemental Materials:

- (1) **Short (ca. <16 cm) bank-top cores from the modern Great Bahama Bank, or GBB** (Romaniello et al., 2013; Zhang et al., 2017). These samples capture initial iodine deposition with primary carbonates from a range of shallow settings and primary mineralogies near Little Darby and Lee Stocking islands (Table 3; Supplementary Figs. 1 and 2).
- (2) **Montastrea annularis coral heads from the Pleistocene Key Largo Limestone, South Florida**. This sample set includes aragonite-to-low-Mg calcite (LMC) transitions driven by sub-aerial exposure and subsequent diagenesis in meteoric pore waters. Post-depositional organic matter remineralization during aragonite-to-calcite neomorphism has resulted in negative  $\delta^{13}\text{C}_{\text{carb}}$  values in some of the LMC samples (Gill et al., 2008).
- (3) **The Neogene–Quaternary Clino and Unda cores, Great Bahama Bank**. These cores were drilled ~8 km apart along the western edge of the Great Bahama Bank (Supplementary Fig. 1). The Clino core contains a negative  $\delta^{13}\text{C}_{\text{carb}}$  excursion in the upper portion reflecting multiple periods of sub-aerial exposure and subsequent aragonite-to-calcite neomorphism in meteoric pore fluids (still ongoing at the top of the core), along with intervals with aragonite-to-calcite neomorphism occurring exclusively in marine pore fluids and minor dolomite, which were all sampled in detail (Melim et al., 1995; Swart and Melim, 2000; Swart and Kennedy, 2012). The Unda and Clino cores have similar depositional histories; however, for the purposes of this study, we did not sample the Unda core in the same stratigraphic detail as the Clino core. For the Unda core, we specifically sampled two intervals of extensive dolomite that formed in exchange with marine pore fluids (Swart and Melim, 2000).
- (4) **Dolomite concretions of the Miocene Monterey Formation, California**. These samples represent dolomite derived mainly from alkalinity production and authigenic carbonate precipitation during remineralization of organic carbon in marine pore fluids, in contrast to recrystallization of carbonate precursors (Loyd et al., 2013).

**Table 3**  
Coordinates, water depth, key depositional features, and mineralogy for cores from near Little Darby and Lee Stocking Islands, Bahamas. Mineralogy is shown in wt.% of high-Mg calcite (HMC). None of the cores contained dolomite and only minor calcite was found in the cores, with HMC+aragonite >93.52 wt.% in all cases, meaning that the sediments mostly consist of aragonite. The detailed mineralogy,  $\delta^{13}\text{C}_{\text{carb}}$ ,  $\delta^{18}\text{O}_{\text{carb}}$ , and I/(Ca+Mg) for each sample can be found in Supplementary Table 1. Also shown is the I/(Ca+Mg) value for uppermost sediment sample and the range for all depths from each short core. Supplementary Fig. 1 contains a map of the sampling localities and Supplementary Fig. 2 shows vertical profiles of I/(Ca+Mg),  $\delta^{13}\text{C}_{\text{carb}}$ , and wt.% aragonite for each of the cores.

Core	Coordinates	Water depth (m)	Key features	HMC (wt.%)	I/(Ca+Mg) ( $\mu\text{mol/mol}$ )	
					Surface	Range
C1	23°51'24.59"N 76°13'30.85"W	<1	intertidal	6.6–23.0	10.2	8.1–10.2
C3	23°51'24.68"N 76°13'33.25"W	<5	subtidal/ <i>Thalassia testudinum</i> bed	15.2–25.6	7.6	6.7–7.6
C4, C6	23°46'11.21"N 76°6'48.92"W	<10	subtidal/former ooid shoal/peloid rich/ <i>Thalassia testudinum</i> bed	13.7–31.3; 8.1–26.5	10.0; 9.4	8.4–10.8; 7.7–9.4
C5	23°45'57.18"N 76°8'3.00"W	<10	subtidal/active ooid shoal/ooid aggregates or grapestones	4.7–9.3	11.6	6.0–11.6
C7	23°46'10.78"N 76°6'51.48"W	<10	subtidal/active ooid shoal/ooid aggregates or grapestones	4.3–10.3	7.2	6.7–7.5
C8	23°51'21.55"N 76°13'33.52"W	<2	subtidal/active ooid shoal/ooid aggregates or grapestones	8.8–24.1	8.2	6.3–8.2

### 3. Methods

Iodine-to-calcium-magnesium ratios and magnesium-to-calcium ratios were measured at Syracuse University using a Bruker M90 quadrupole inductively-coupled-plasma mass spectrometer (ICP-MS) and at the University of California, Riverside, using a Agilent 7900c ICP-MS, according to standard methods (Hardisty et al., 2014; Lu et al., 2010, 2016; Zhou et al., 2014, 2015). All samples from the Clino and Unda cores and the Monterey and Tieling formations were measured at UC Riverside and the remainder at Syracuse University. Approximately 3–5 mg of powdered carbonate was used for each analysis. Samples were sonicated in 1 mL DI water that was then centrifuged and decanted. Following this, 3%  $\text{HNO}_3$  was added to each sample allowing for complete dissolution of all carbonate, and these were similarly sonicated for ~10 minutes and centrifuged. The supernatant was diluted in a matrix with combinations of nitric acid and an iodine-stabilizing solution (tertiary amine or tetramethyl ammonium hydroxide) to obtain Ca concentrations of approximately 50 ppm. Calibration standards were made fresh each day from powdered potassium iodate in a similar matrix with the addition of 50 ppm Ca. The coral standard JCP-1 was analyzed intermittently with average values at Syracuse University and UC Riverside that were identical within error.

The mineralogical determinations for the Clino and Unda cores, Monterey, Key Largo, and Bahamas Bank top cores were performed at the University of Miami using a Panalytical X-Pert Pro via a method published previously (Melim et al., 1995). The associated error is  $\pm 2$  wt.%. Carbon and oxygen isotope values for the Johnnie Formation, the Clino and Unda cores, and portions of the GBB short cores were measured at the University of California, Riverside, using a GasBench II interface coupled, via continuous flow, to a Delta V Thermo Advantage IRMS (Isotope Ratio Mass Spectrometer). Carbon and oxygen isotope values for the C1, C4, C6, and C7 Bahamas Bank top cores were analyzed at The Center for Stable Isotope Biogeochemistry at UC, Berkeley, using a MultiCarb system connected with a GV IsoPrime mass spectrometer in dual inlet mode. Carbon and oxygen isotopes for the Doushantuo Formation were measured at the University of Nevada, Las Vegas, using a Kiel IV carbonate device connected to a Finnigan Delta V Plus mass spectrometer in dual inlet mode. All values are presented in the standard delta notation as per mil (‰) deviation from Vienna Pee Dee Belemnite (V-PDB), with replicate standard analyses yielding standard deviations typically better than 0.10‰ for carbon and oxygen isotopes.

### 4. Results

The highest I/(Ca+Mg) values in our Neogene–Quaternary samples, ranging from 6.0–11.6  $\mu\text{mol/mol}$ , are found in predominantly aragonite and HMC samples from bank-top cores from the well-oxygenated GBB (Table 3). The Key Largo coral heads contain I/(Ca+Mg) values that show little change across the meteoric fluid-driven aragonite-to-calcite mineralogy transition, with only KL-11 containing samples with decreased iodine contents in some, but not all, LMC-dominated samples (Fig. 2). For cores Clino and Unda, the carbon and oxygen isotopic and mineralogical trends and values within specific intervals are generally consistent with that of previous work of different samples from the same core (e.g., Melim et al., 1995; Swart and Melim, 2000; Swart and Kennedy, 2012), including the negative  $\delta^{13}\text{C}_{\text{carb}}$  excursion characterizing the meteoric zone in the Clino core (Fig. 3). The Clino core contains I/(Ca+Mg) ranging from below detection to 5.71  $\mu\text{mol/mol}$ . The highest I/(Ca+Mg) values overlap with intervals containing relatively higher aragonite content, with most LMC- and dolomite-dominated intervals generally containing relatively lower I/(Ca+Mg) ratios (Fig. 4). The Unda and Monterey samples have I/(Ca+Mg) values ranging from below detection to 0.46 and 1.01  $\mu\text{mol/mol}$ , respectively (Fig. 4). Of the samples containing greater than 20 wt.% dolomite, I/(Ca+Mg) ratios are <0.46 and 0.40  $\mu\text{mol/mol}$  for the Monterey Formation and the Unda core, respectively, with most values below detection.

Our Proterozoic samples contain both dolomite and limestone (Fig. 5), and iodine is present in some of the samples from nearly all the units evaluated (Fig. 6). Proterozoic I/(Ca+Mg) ratios from carbonates older than the late Ediacaran Shuram anomaly are  $\leq 2.8$   $\mu\text{mol/mol}$  and are often much less—notably within the range observed in primary carbonate from modern low-oxygen settings (yellow squares, Fig. 6). There is a drop in maximum I/(Ca+Mg) to  $\leq 0.8$   $\mu\text{mol/mol}$  around ~2.0 Ga, following the Lomagundi positive carbon isotope excursion (LE; ~2.2–2.1 Ga). In the following interval, from 2.0 to 1.0 Ga, maximum values of  $\leq 0.8$   $\mu\text{mol/mol}$  are found in 13 of the 14 studied units with the only exception being the Tieling Formation of North China, where maximum I/(Ca+Mg) ratios are similar to those characterizing the LE and early Neoproterozoic (Fig. 6). Starting at roughly 1.0 Ga, maximum values are more frequently elevated relative to the mid-Proterozoic. Lastly, all four of our Ediacaran, Shuram-age sections show a marked increase in I/(Ca+Mg) in phase with the dramatic decrease in  $\delta^{13}\text{C}_{\text{carb}}$  (Fig. 7).

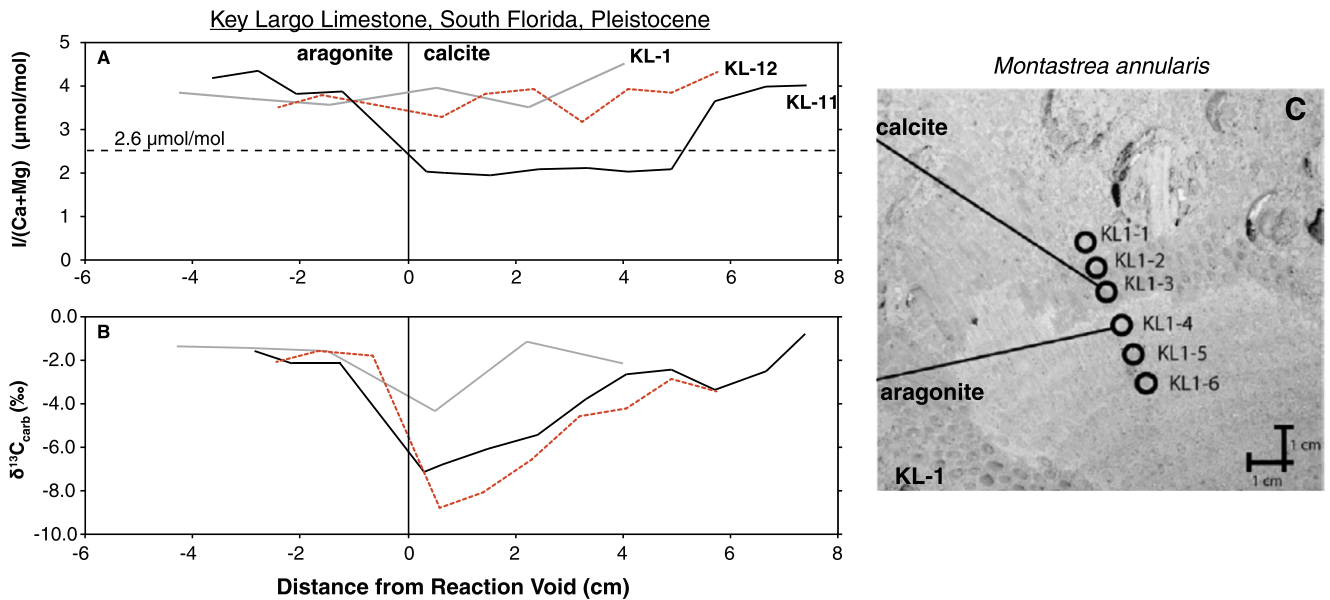


**Fig. 2.** (a)  $I/(Ca+Mg)$  and (b)  $\delta^{13}C_{carb}$  for transects through three aragonite-dominated to calcite-dominated portions of (c) *Montastrea annularis* coral heads of the Pleistocene Key Largo Limestone of South Florida. The samples and transects are exactly the same as those used in Gill et al. (2008). The horizontal dashed line at 2.6  $\mu\text{mol/mol}$  (part a) represents the  $I/(Ca+Mg)$  ratio range found in calcitic forams from low oxygen water column settings (Glock et al., 2014; Lu et al., 2016). A picture of the KL-1 coral head and drilled transect is shown in part c as an example, with the circles representing discrete sampling locations. The transect is drilled at centimeter intervals across a mineralogical transition from aragonite to calcite driven by subaerial exposure and diagenesis in meteoric pore fluids. The aragonite can be discerned by the lighter color and the calcite by the darker color, with the reaction void occurring between KL1-3 and KL1-4. Scale bar in bottom right hand corner is 1 cm.

## 5. Discussion

### 5.1. Iodine behavior in response to Neogene–Quaternary carbonate diagenesis

No previous study has measured carbonate iodine contents within an independently established framework of well-constrained diagenetic alteration. Interpretation of iodine contents of water column-derived calcitic foraminifera is obviously ideal; however, this is not always possible in ancient samples. Multiple previous studies have instead measured bulk iodine in ancient carbonate (Hardisty et al., 2014; Loope et al., 2013; Zhou et al., 2015; Owens et al., 2017). Below we provide a context for interpreting our Proterozoic bulk carbonate data through a process-oriented perspective in Neogene–Quaternary carbonate of the Bahamas and Monterey Formation that progresses from modern carbonate precipitation to deposition, burial, and subsequent variable styles of diagenetic mineral transformation. With the exception of the Monterey Formation, the waters that hosted primary carbonate precipitation are constrained to have been well oxygenated, which implies that presently low and highly variable  $I/(Ca+Mg)$  ratios do not record shifts in the  $IO_3^-$  content of the local waters of deposition. Instead, low  $I/(Ca+Mg)$  values or variations likely track secondary processes related to depositional setting, mineralogy, and related diagenetic overprinting of primary values.

The highest  $I/(Ca+Mg)$  ratios in our Neogene–Quaternary sample set come from the GBB bank-top cores (Table 3), which is the least altered sample set of this study and representative of the carbonate iodine signature of initial deposition. The range in  $I/(Ca+Mg)$  values from bulk aragonite-HMC in all the GBB bank-top core samples (6.0–11.6  $\mu\text{mol/mol}$ ; Table 3) is higher than that found in LMC foraminifera, which in previous studies of well-oxygenated settings spans from 4–7  $\mu\text{mol/mol}$  (Lu et al., 2016). None of our  $I/(Ca+Mg)$  profiles from any of the seven GBB short cores increases with depth (Table 3; Supplementary Fig. 2), indicating that the elevated  $I/(Ca+Mg)$  values are unrelated to post-burial processes. Uncertainties surrounding partition coefficients for HMC and aragonite relative to that of calcite and potential vital effects

associated with uncharacterized skeletal debris may lead to errors in the estimated  $IO_3^-$  content of ambient waters from variable carbonate mineralogies. Until the partition coefficients of iodine for individual carbonate mineralogies are resolved, caution should be taken in comparing absolute  $I/(Ca+Mg)$  ratios between samples of mixed or unknown carbonate mineralogy. For example, if we apply the partition coefficients from laboratory LMC precipitation experiments (Lu et al., 2010; Zhou et al., 2014) to the  $I/(Ca+Mg)$  ratios from our aragonite- and HMC-dominated GBB carbonate, we predict local marine  $IO_3^-$  abundance from  $\sim 600$  nM to approaching 1  $\mu\text{M}$ , which is not consistent with the typical range observed in marine, surface waters (roughly 300 to 450 nM; Chance et al., 2014). However, the wide and elevated range in  $I/(Ca+Mg)$  from the GBB is not easily attributed to any one factor, as the GBB  $I/(Ca+Mg)$  ratios differ even between adjacent oolitic shoals of similar composition and show no clear co-variation with mineralogy,  $\delta^{13}C_{carb}$ , or modern depositional setting (Table 3; Supplementary Fig. 2). Regardless, our observations are consistent with previous works indicating that the  $I/(Ca+Mg)$  ratios of primary carbonate minerals precipitated from well-oxygenated seawater do not overlap with the 0–2.6  $\mu\text{mol/mol}$  values observed for calcitic foraminifera living within low-oxygen settings (Glock et al., 2014; Lu et al., 2016).

The Key Largo coral heads provide a case study specific to initial aragonite precipitation and post-depositional meteoric aragonite-to-calcite neomorphism during subaerial carbonate exposure (Gill et al., 2008). In this case, the  $I/(Ca+Mg)$  ratios of primary aragonite fall within the range reported for LMC foraminifera from well-oxygenated settings (Fig. 2). Previous work from these same samples has shown that lower dissolved elemental abundances (e.g., S, Sr) in fresh (meteoric) waters versus seawater, which to a lesser extent is also true of iodine (Fehn, 2012), lead to decreases in their concentrations in diagenetic LMC relative to primary aragonite (Gill et al., 2008). Opposite of this expectation, however, the primary  $I/(Ca+Mg)$  ratios generally change little across the aragonite-to-calcite transitions of our samples. The only exception is a LMC interval directly at the reaction front of KL-11 that contains lower  $I/(Ca+Mg)$  relative to the primary aragonite (Fig. 2),

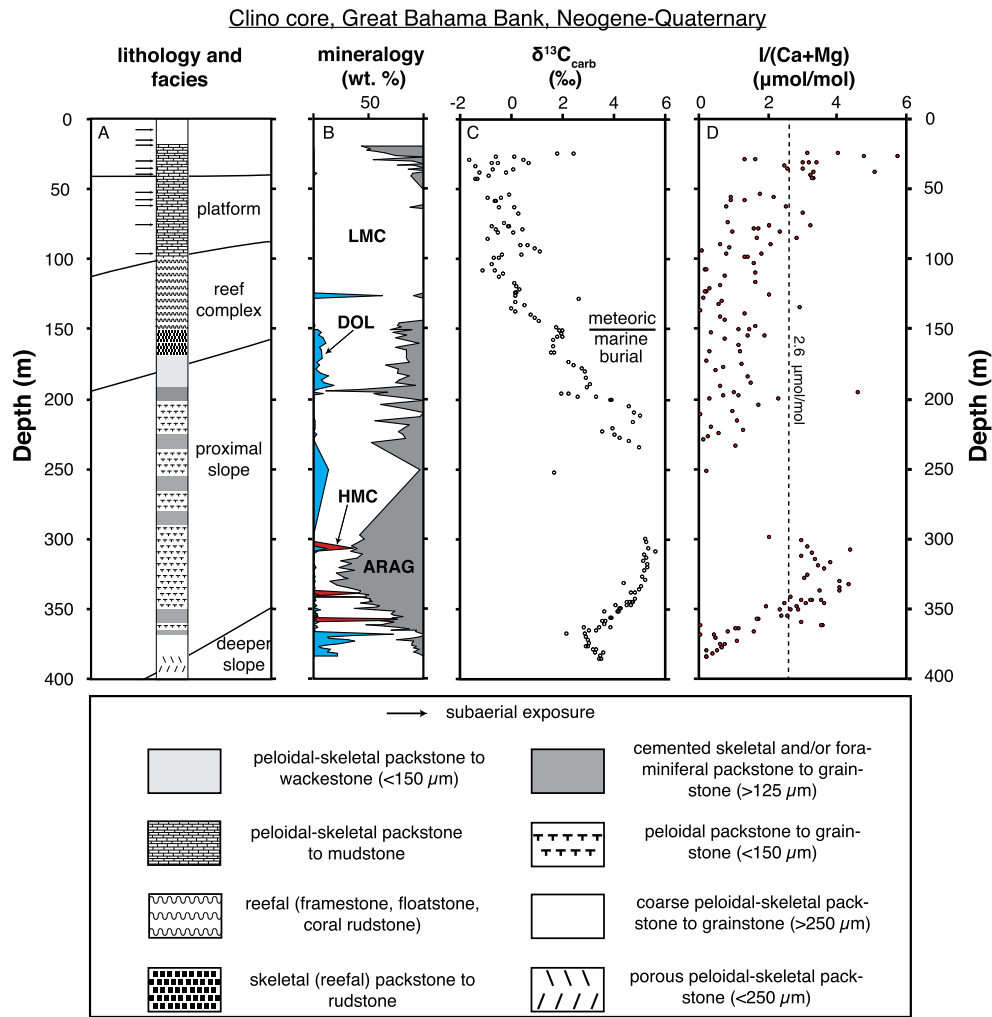


**Fig. 3.** The (a) facies and lithology (horizontal and slanted lines represent ramp paleo geometry; Swart and Melim, 2000), (b) carbonate mineralogy (aragonite–dark grey; HMC–red, LMC–white; dolomite–blue), (c)  $\delta^{13}\text{C}_{\text{carb}}$ , and (d)  $\text{I}/(\text{Ca}+\text{Mg})$  ratios for the Clino core of the Great Bahama Bank. Lithological descriptions come from Kenter et al. (2001) and Manfrino and Ginsburg (2001). The vertical dashed line at 2.6  $\mu\text{mol}/\text{mol}$  represents the  $\text{I}/(\text{Ca}+\text{Mg})$  ratio range found in calcitic forams from low oxygen water column settings (Glock et al., 2014; Lu et al., 2016). (For interpretation of the references to color in this figure legend, the reader is referred to the web version of this article.)

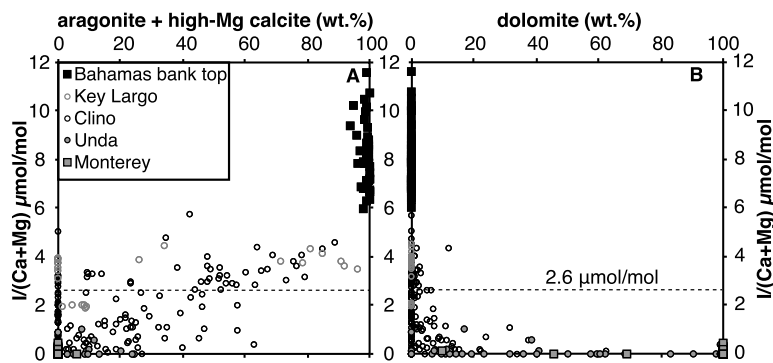


**Fig. 4.** The composition of (a) primary aragonite and high-Mg calcite and (b) diagenetic dolomite relative to  $\text{I}/(\text{Ca}+\text{Mg})$  ratios for the diagenetic sample set described in the main text and labeled in the legend. The horizontal dashed line is at an  $\text{I}/(\text{Ca}+\text{Mg})$  of 2.6  $\mu\text{mol}/\text{mol}$ , the threshold, which, as discussed in the text, is characteristic of reducing marine setting (Glock et al., 2014; Lu et al., 2016).

but there are no discernable differences between these and other LMC samples with relatively elevated  $\text{I}/(\text{Ca}+\text{Mg})$ . The maintenance of high, primary  $\text{I}/(\text{Ca}+\text{Mg})$  ratios during meteoric diagenesis in the Key Largo samples may represent a special case where oxic diagenetic conditions allowed for the iodine content of the primary aragonite to (at least temporarily) buffer iodine contents of the diagenetic LMC. Sulfate reduction is known to partially pro-

note aragonite-to-calcite neomorphism during meteoric diagenesis in the Bahamas (McClain et al., 1992)—conditions where iodine would be present primarily as  $\text{I}^-$ . However, the  $\delta^{34}\text{S}$  values of carbonate-associated sulfate (CAS) in both our original aragonite and secondary LMC Key Largo samples are similar to those of Pleistocene/modern seawater sulfate (Gill et al., 2008), arguing against substantial sulfate reduction during meteoric diagenesis. Nonethe-

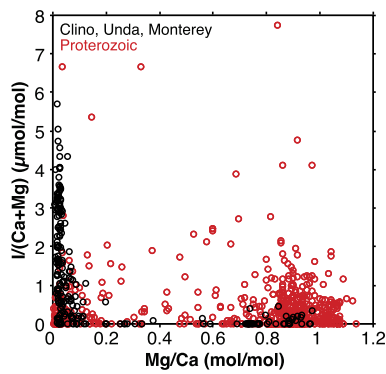


**Fig. 5.** Comparison of  $I/(Ca+Mg)$  to  $Mg/Ca$  for the Neogene dolomite-bearing sample sets from this study relative to the Proterozoic sample set from this and previous Proterozoic studies (Hardisty et al., 2014).

less, the Key Largo profiles support that  $I/(Ca+Mg)$  ratios have the potential to be maintained, but are unlikely to increase following deposition and neomorphism driven by diagenesis in meteoric fluids.

The Clino core best illustrates the range in diagenetic zones and related geochemical and mineralogical variability possible from the GBB (Figs. 3, 4). The diagenetic zones reflect a temporal transition from a slope to a platform depositional setting during the Neogene–Quaternary, with a negative  $\delta^{13}C_{carb}$  excursion in the upper portion due to multiple periods of subaerial exposure and subsequent aragonite-to-calcite neomorphism within meteoric fluids (Melim et al., 1995; Swart and Melim, 2000). Below this depth, aragonite-to-calcite neomorphism and minor dolomitization occurred exclusively in marine pore waters (Melim et al., 1995; Swart and Melim, 2000). The  $I/(Ca+Mg)$  ratios from the aragonite-HMC GBB short cores and aragonitic portions of the Key Largo Limestone are most like those expected for primary  $I/(Ca+Mg)$  ra-

tios from the Bahamian Clino core (i.e.,  $I/(Ca+Mg) > 3 \mu\text{mol/mol}$ ). Indeed, although the Clino core sample set no longer contains intervals with 100% aragonite and has only sparse HMC, the samples with higher aragonite contents do generally contain the  $I/(Ca+Mg)$  ratios that are above those observed from low-oxygen depositional settings (Figs. 3, 4a). However, the core shows clear diagenetic iodine loss in secondary LMC and dolomite phases, as most of the Clino core  $I/(Ca+Mg)$  ratios overlap with the  $< 2.6 \mu\text{mol/mol}$  values observed from low-oxygen marine settings. The ratios show no distinct trends with  $\delta^{13}C_{carb}$ , with regard to diagenetic zones, specific to lithology, or across the facies transitions (Fig. 3). Instead, the inferred decreases in  $I/(Ca+Mg)$  ratios during diagenesis in the Clino core are consistent with previous inferences for neomorphism of aragonite and HMC to LMC and dolomite in pore waters hosting significant sulfate reduction and closed to seawater exchange (Swart and Melim, 2000). Despite initial deposition in a well-oxygenated setting with temporally varying facies likely hosting a large array of high primary  $I/(Ca+Mg)$  ratios, we surmise that progressive diagenesis will ultimately decrease ratios to relatively low values within a small range for the entire core. This includes the currently high  $I/(Ca+Mg)$  values in the aragonitic intervals near the top and bottom of our sampled profile. These observations imply that there is likely much overlap between ranges in  $I/(Ca+Mg)$  from carbonate precipitated from low oxygen and anoxic water columns and secondary carbonate phases precipitated in low oxygen or anoxic pore waters (Fig. 3d). When possible, measurement of  $I/(Ca+Mg)$  from calcite with independent constraints as representing primary carbonate phases will be ideal.

The samples from the Unda core and Monterey concretions were specifically selected to provide constraints on iodine contents in dolomites that are well constrained to have precipitated within marine pore waters (Fig. 4b). Our samples from the Unda core contain 100% dolomite in many cases, which previous studies have linked to reefal sediments that experienced aragonite-to-LMC neomorphism in marine pore fluids prior to dolomitization

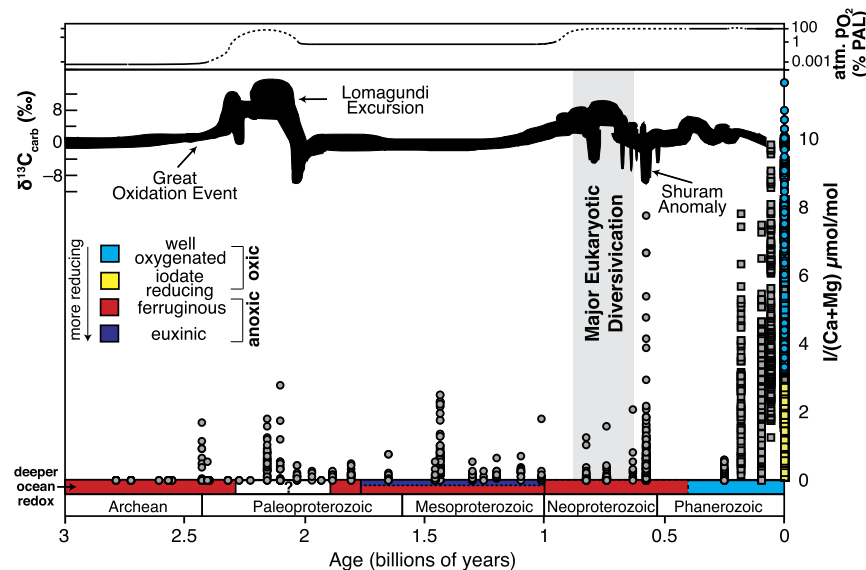


**Fig. 6.** Compilation of proxy data distinguishing the redox state of the atmosphere (upper panel), surface ocean (middle panel), and deeper ocean (lower panel). Events discussed in the text are labeled, including the period when the major eukaryotic diversification took place (vertical gray bar; from Knoll, 2014). Upper panel: The secular trend in atmospheric oxygen as discussed in recent compilations (Lyons et al., 2014; Planavsky et al., 2014). Dashed lines in the upper panel represent uncertainty due to a lack of quantitative constraints. Middle panel:  $\delta^{13}C_{carb}$  (upper thick black line) and  $I/(Ca+Mg)$  (Glock et al., 2014; Hardisty et al., 2014; Loope et al., 2013; Lu et al., 2010, 2016; Zhou et al., 2014, 2015).  $I/(Ca+Mg)$  ratios reflect surface ocean redox conditions. Blue symbols on the right side represent samples from modern to recent settings with independent evidence for a well-oxygenated water column and lacking indicators of diagenetic overprinting. This includes foraminifera (Lu et al., 2016), aragonitic coral heads of the Key Largo Limestone from this study, and aragonite- to HMC-dominated bulk carbonate from the modern Great Bahama Bank of this study. The yellow symbols correspond to modern foraminifera from within the oxycline of reducing settings (Glock et al., 2014; Lu et al., 2016). The square symbols indicate data representing  $I/Ca$  from calcitic foraminifera, equivalent to  $I/(Ca+Mg)$  in the case of calcite. Bottom panel: Generalized deep-ocean redox, as inferred from previous work utilizing iron mineral speciation (Sperling et al., 2015). Red and purple boxes represent ferruginous and euxinic deep-marine waters, respectively. (For interpretation of the references to color in this figure legend, the reader is referred to the web version of this article.)

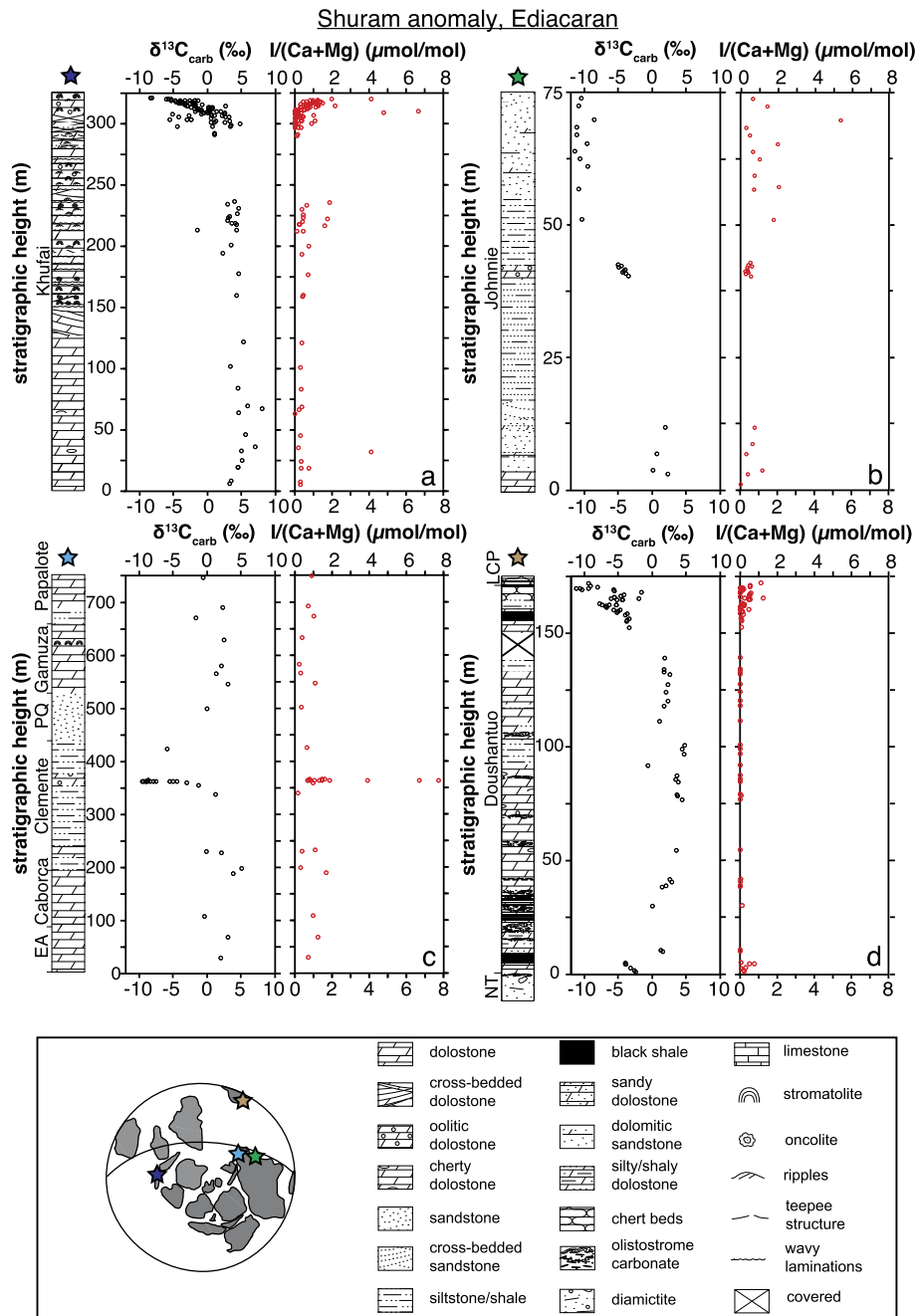


**Fig. 7.** The  $\delta^{13}\text{C}_{\text{carb}}$ ,  $I/(\text{Ca}+\text{Mg})$  ratios, and stratigraphic profiles for Ediacaran successions capturing the Shuram anomaly: (a) Khufai Formation, Oman ( $\delta^{13}\text{C}_{\text{carb}}$  and stratigraphy from Osburn et al., 2015), (b) the Johnnie Formation, Death Valley, USA, (c) Clemente Formation, Northern Mexico ( $\delta^{13}\text{C}_{\text{carb}}$  and stratigraphy from Loyd et al., 2013), and (d) Doushantuo Formation, Siduping of South China.  $1\sigma$  for  $I/(\text{Ca}+\text{Mg})$  is equal to  $0.2 \mu\text{mol/mol}$  (see Methods), twice the width of the data points. The Ediacaran paleogeographic reconstruction is adapted from Pisarevsky et al. (2008).

(Swart and Melim, 2000). Dolomite concretions of the Monterey Formation were largely not derived from neomorphism of primary marine carbonate. Instead, they represent authigenic dolomite precipitated in phase with extensive pore water alkalinity production during remineralization in organic-rich sediments marked by anoxic pore fluids closed to exchange with seawater (Blättler et al., 2015; Loyd et al., 2012). Despite the very different mechanisms of dolomite precipitation, the two diagenetic dolomite sample sets reveal similar results, yielding the lowest  $I/(\text{Ca}+\text{Mg})$  ratios of our entire diagenetic data set. Most values are below detection, and the highest value is  $0.46 \mu\text{mol/mol}$ . We suggest that the extremely low values reflect multiple generations of diagenetic mineral transformation for dolomites of the Unda core and anoxic diagenetic

conditions in both cases. The presence of iodine in some Monterey dolomite samples may indicate minor contributions from recrystallization of primary carbonate that initially contained some iodine. The low  $I/(\text{Ca}+\text{Mg})$  values from both dolomite sample sets are not likely to completely reflect differences in partition coefficients for dolomite relative to LMC (though this has yet to be resolved), as many Proterozoic dolomites from this study have high ratios relative to the Neogene sample set (discussed in the next section; Fig. 5). Ultimately, our results reveal that dolomitization of carbonate precursors and authigenic dolomite precipitation in marine pore fluids will dramatically lower  $I/(\text{Ca}+\text{Mg})$  ratios from that characteristic of primary carbonate formed in well-oxygenated water columns. Without proper caution, low dolomite ratios could

lead to underestimation of  $\text{IO}_3^-$  and hence the  $\text{O}_2$  availability in the overlying water column. In carbonates characterized by ubiquitous dolomite, independent geochemical constraints on the redox state (e.g.,  $\delta^{34}\text{S}_{\text{CAS}}$ ) and the extent of exchange with seawater (e.g., Ca and Mg isotopes) during dolomite precipitation may provide the most ideal context for determining the confidence in which  $\text{I}/(\text{Ca}+\text{Mg})$  ratios reflect water column or diagenetic chemistry.

### 5.2. Neogene–Quaternary perspectives on Proterozoic carbonate diagenesis

Our proxy validation efforts with the Neogene–Quaternary samples indicate that  $\text{I}/(\text{Ca}+\text{Mg})$  ratios should not increase during diagenesis in reducing pore fluids. Given this observation, the simple presence of iodine in ancient carbonate is a robust fingerprint of oxic conditions. Again, ‘false positives’ are not anticipated and have not been observed in young sediments. Iodine’s redox behavior distinguishes it from other common paleoredox proxies (e.g., Fe speciation, S isotopes and concentrations, and Mo and U concentrations), which specifically fingerprint local anoxic water columns and are most commonly applied to deeper basinal shales. Beyond the simple presence–absence of surface ocean  $\text{O}_2$ , detailed comparison of Proterozoic  $\text{I}/(\text{Ca}+\text{Mg})$  trends to Neogene–Quaternary diagenetic carbonate and dolomite support that Proterozoic temporal trends may reflect seawater redox evolution, including relative changes in the depth of anoxic waters relative to that of carbonate precipitation, when interpreted with appropriate caution. For instance, there are no known temporal variations in diagenesis that would cause the observed first-order, long-term patterns through the Precambrian and preferentially favor the persistence of generally low maximum values during the mid-Proterozoic and the absence of iodine in Archean samples (Fig. 6).

An additional, valuable case study in our effort to distinguish seawater versus pore water origins for Proterozoic  $\text{I}/(\text{Ca}+\text{Mg})$  signal comes from a comparison between the  $\text{I}/(\text{Ca}+\text{Mg})$  trends spanning the Shuram negative  $\delta^{13}\text{C}_{\text{carb}}$  anomaly (Fig. 7) and our sample set recording Neogene–Quaternary diagenesis, most notably that linked to the negative  $\delta^{13}\text{C}_{\text{carb}}$  values of the Clino core (Fig. 3). Both meteoric and marine diagenesis have been invoked to explain the extremely negative  $\delta^{13}\text{C}_{\text{carb}}$  values of the Shuram anomaly and other negative Neoproterozoic  $\delta^{13}\text{C}_{\text{carb}}$  excursions (Schrag et al., 2013; Swart and Kennedy, 2012), with the Shuram carbon isotope values trending from +5 to  $-12\%$  (Fig. 7). The meteorically driven negative  $\delta^{13}\text{C}_{\text{carb}}$  excursion of the Clino core has specifically been invoked to suggest the possibility that ancient negative  $\delta^{13}\text{C}_{\text{carb}}$  excursions are products of diagenesis rather than secular evolution of the global carbon cycle (Swart and Kennedy, 2012). If diagenetic, the Shuram  $\delta^{13}\text{C}_{\text{carb}}$  data would most likely reflect post-depositional mineralogical transformations and the associated low  $\delta^{13}\text{C}$  values of dissolved inorganic carbon produced in pore fluids during organic matter remineralization under anoxic or reducing subsurface conditions. Our iodine data from the Clino core and other Neogene–Quaternary sediments confirm that  $\text{I}/(\text{Ca}+\text{Mg})$  values do not increase during diagenesis and show no relationship with  $\delta^{13}\text{C}_{\text{carb}}$  (Fig. 2), as  $\text{IO}_3^-$  is quantitatively reduced under the anoxic conditions typical of diagenetic carbonate precipitation (Kennedy and Elderfield, 1987a, 1987b). In contrast, however,  $\text{I}/(\text{Ca}+\text{Mg})$  ratios across the Shuram excursion, at each of our four paleogeographically distant localities, increase in parallel with decreasing  $\delta^{13}\text{C}_{\text{carb}}$  values and do so consistently despite variable mineralogy and sedimentary facies (Fig. 7). Notably, the maximum observed  $\text{I}/(\text{Ca}+\text{Mg})$  ratios vary among the Shuram sections, which could be the result of spatially variable, redox-driven local water column  $\text{IO}_3^-$  concentrations or a range of secondary factors that can lower the values in different ways (see diagenesis discussion). Regardless, the observed stratigraphic increase in

$\text{I}/(\text{Ca}+\text{Mg})$  ratios at all four locations in phase with the falling  $\delta^{13}\text{C}_{\text{carb}}$  limb of the Shuram anomaly is the opposite of the pattern expected with diagenesis (Figs. 2, 3, 4). Collectively, these data support the likelihood that the Shuram anomaly at least partially captures local seawater availability of  $\text{IO}_3^-$  and is a primary  $\delta^{13}\text{C}$  feature tracking trends, likely global, in seawater chemistry. A primary contribution to the Shuram anomaly is further braced by records of CAS (Kaufman et al., 2007; Loyd et al., 2013; Osburn et al., 2015), U concentrations (Zhao et al., 2016), detailed Ca–Mg–C isotope comparisons (Husson et al., 2015), and compound-specific  $\delta^{13}\text{C}$  values of organic carbon (Lee et al., 2015), all of which show trends counter to those expected from diagenetic alteration.

Lastly, dolomitization in Proterozoic samples is not necessarily a source of false secular trends or, more generally, a fingerprint of severely altered samples not recording signals of primary ocean chemistry. Instead, previous workers have argued from a combination of retention of primary sedimentary fabrics (Fairchild et al., 1991; Kah, 2000; Tucker, 1982), geochemical data (Husson et al., 2015; Kah, 2000; Tucker, 1982), and petrographic evidence (Tucker, 1982; van Smeerdijk Hood et al., 2011) that many dolomites formed penecontemporaneously with deposition in the Proterozoic, in open exchange with seawater, and potentially at or near the sediment–water interface. We do acknowledge that stoichiometrically disordered dolomite is subject to continued maturation during diagenesis (Vahrenkamp and Swart, 1994). Still, one implication is that the long-term stability of dolomite relative to other carbonate phases could mean that Proterozoic early diagenetic dolomite, even if replacive, may be a stronger and even preferred geochemical archive of ancient marine conditions relative to stratigraphically associated limestone subject to diagenetic alteration during neomorphism. A comparison of iodine data from our Neogene diagenetic dolomite from the Bahamas and Monterey to Proterozoic samples further reinforces the potential frequency and benefit of early Proterozoic dolomite and points to processes regulating  $\text{I}/(\text{Ca}+\text{Mg})$  ratios other than dolomitization in some of our samples (Fig. 5). Specifically, the highest  $\text{I}/(\text{Ca}+\text{Mg})$  ratios from our Proterozoic carbonates are found often in dolomite—a trend opposite to that seen in our Neogene samples. Late-stage diagenetic processes, such as interaction with anoxic brines (e.g., Derry, 2010), provide an unlikely explanation for the elevated  $\text{I}/(\text{Ca}+\text{Mg})$  ratios in our Proterozoic dolomite, as these fluids would not support elevated  $\text{IO}_3^-$  contents. Given the early redox sensitivity of  $\text{IO}_3^-$  reduction with declining  $[\text{O}_2]$ , our data reinforce the idea that in some cases Proterozoic dolomite precipitation likely occurred near or at the sediment–water interface and hence should record at least partial seawater signals (cf., Fairchild et al., 1991; Kah, 2000; Tucker, 1982; van Smeerdijk Hood et al., 2011).

Given the combination of observations here and in previous work, broad first-order temporal trends in maximum  $\text{I}/(\text{Ca}+\text{Mg})$  ratios are cautiously considered in discussions below as records of shallow ocean redox evolution. We emphasize again that our combined diagenetic data explicitly reveal that post-depositional increases in  $\text{I}/(\text{Ca}+\text{Mg})$  are unlikely, and hence, if anything, the maximum  $\text{I}/(\text{Ca}+\text{Mg})$  value from a given section is a minimum estimate of local seawater  $\text{IO}_3^-$  availability. While we are not linking  $\text{I}/(\text{Ca}+\text{Mg})$  ratios to a specific seawater  $\text{IO}_3^-$  concentration, we do maintain that the first-order trends over billions of years are difficult to attribute to secondary effects.

### 5.3. Comparing the modern and Proterozoic marine iodine reservoir

Our temporal  $\text{I}/(\text{Ca}+\text{Mg})$  record in Fig. 6 suggests the likelihood of changes in marine  $\text{IO}_3^-$  concentrations through time. Modern settings indicate that the control responsible for the largest shifts in local marine  $\text{IO}_3^-$  concentration is the local redox state (Fig. 1;

Emerson et al., 1979; Farrenkopf and Luther III, 2002; Rue et al., 1997; Wong and Brewer, 1977); however, changes in the size of the total marine dissolved iodine reservoir (both  $\text{IO}_3^-$  and  $\text{I}^-$ ) could also control  $\text{IO}_3^-$  concentrations if oxic conditions prevailed. We consider this possibility below.

The Precambrian iodine reservoir was likely larger than today's or, more generally, that of the Phanerozoic as a whole due to the absence or limited role of algal primary production and burial in marine sediments during the Precambrian. Marine sediments and sedimentary rocks are estimated to host as much as ~96% of crustal iodine, with the remaining fraction present in the hydrosphere and igneous and metamorphic rocks (Muramatsu and Wedepohl, 1998). Algae, particularly brown algae, host the largest iodine enrichments in any known natural material by orders of magnitude, significantly contributing to iodine enrichment in organic-rich sediments (Muramatsu and Wedepohl, 1998), which is recycled back to the ocean during weathering, diagenesis, and subduction (Fehn, 2012; Lu et al., 2010). Importantly, the first fossil evidence for algae does not appear until the late Mesoproterozoic (reviewed in Knoll, 2014), and records of algal-derived sterane biomarkers—representing eukaryotes—do not support algae being dominant contributors to marine organic matter until the latest Proterozoic (e.g., Brocks et al., 2016). Relatively small iodine sinks in both Proterozoic sedimentary organic matter and carbonate (see Fig. 6) point to a likely larger Proterozoic seawater iodine reservoir relative to today. These observations imply that our finding of low  $\text{I}/(\text{Ca}+\text{Mg})$  in the Precambrian relative to the modern carbonates is unlikely to reflect a smaller marine reservoir of total dissolved iodine or shifts in that pool, but instead derive from lower marine  $\text{IO}_3^-$  concentrations at the site of carbonate precipitation related primarily to local redox.

For the Shuram anomaly specifically, we speculate that the oxidation of algae-derived organic matter could drive a temporally isolated increase in the total dissolved marine iodine reservoir. Oxidation of organic matter, as suggested in previous studies (Rothman et al., 2003; Fike et al., 2006; Kaufman et al., 2007), also provides a mechanism for the input of isotopically light DIC into the ocean to produce the negative  $\delta^{13}\text{C}_{\text{carb}}$  characteristic of the Shuram excursion. For instance, simple mass balance calculations suggest that the input of DIC from organic carbon oxidation (with a  $\delta^{13}\text{C}$  of  $-25\text{‰}$ ) necessary to drive a whole-ocean  $-17\text{‰}$   $\delta^{13}\text{C}$  excursion (equivalent to that often inferred for the Shuram anomaly) in the modern ocean would increase the total marine dissolved iodine reservoir by a factor of ~1.6 (using the typical algae  $\text{I}/\text{TOC}$  ratio of  $10^{-4}$ ). However, given that  $\text{I}/(\text{Ca}+\text{Mg})$  tracks  $\text{IO}_3^-$  and not total iodine, it is unlikely that the Shuram increase in  $\text{I}/(\text{Ca}+\text{Mg})$  is simply a product of an increase in the total marine iodine reservoir. For example, regardless of an increase in the total iodine reservoir,  $\text{IO}_3^-$  concentrations (and hence  $\text{I}/(\text{Ca}+\text{Mg})$  ratios) would decrease (the opposite of what is observed) during the excursion if oxidation of reduced carbon acted to simultaneously expand anoxia (Lu et al., 2010; Zhou et al., 2015). We suggest instead that an increase in marine  $\text{IO}_3^-$  through the Shuram anomaly would also require an expansion of oxic settings at least in the shallow ocean. Supporting this, S concentrations and isotope data for CAS through the Shuram anomaly provide evidence for an increase in marine sulfate concentrations and hence a general expansion of oxidizing conditions in the same settings recording increased  $\text{IO}_3^-$  abundance from  $\text{I}/(\text{Ca}+\text{Mg})$  ratios (Fike et al., 2006; Kaufman et al., 2007; Loyd et al., 2013; Osburn et al., 2015). Importantly, however, our iodine data do not demand that an oxidation event driving the negative  $\delta^{13}\text{C}_{\text{carb}}$  excursion was linked to deep ocean ventilation. Oxygenation may instead have been limited to near-surface settings. Redox stratification through the Shuram anomaly is supported by decreased  $\text{I}/(\text{Ca}+\text{Mg})$  ratios following the event and thus an inferred return to more reducing conditions

in the ocean (Fig. 7c), geochemical studies suggesting widespread anoxia before and after the excursion (e.g., Johnston et al., 2013; Sperling et al., 2015), as well as mass balance calculations highlighting the challenges of maintaining the oxidants necessary to drive the  $\delta^{13}\text{C}$  excursion if it reflects whole-ocean ventilation (Bristow and Kennedy, 2008). Explaining the origin of the Shuram  $\delta^{13}\text{C}_{\text{carb}}$  excursion remains a challenge; however, future models should consider the growing evidence for spatiotemporally limited oxidation specific to shallow settings at the onset of the excursion.

#### 5.4. Proterozoic surface ocean redox

In light of our study of diagenetic effects in recent carbonates, the simple presence of iodine in most of the Proterozoic carbonate units we analyzed provides strong evidence for surface ocean  $[\text{O}_2]$  above the low threshold required for  $\text{IO}_3^-$  accumulation. Previous studies have argued for an  $[\text{O}_2]$  requirement of at least 1–3  $\mu\text{M}$  for marine  $\text{IO}_3^-$  accumulation and the presence of carbonate-bound iodine (Hardisty et al., 2014). Further support for Proterozoic surface ocean  $[\text{O}_2]$  at or above low  $\mu\text{M}$  levels comes from the fossil evidence for the presence of eukaryotic microfossils in mid-Proterozoic oceans (Knoll, 2014), as well as from modeling efforts indicating the potential for single digit  $\mu\text{M}$  surface ocean  $\text{O}_2$  concentrations from *in situ* oxygenic photosynthesis under even a completely anoxic atmosphere (Reinhard et al., 2016). Importantly, the >1–3  $\mu\text{M}$   $\text{O}_2$  levels inferred for the Proterozoic surface ocean are above those predicted from equilibrium calculations, assuming the very low mid-Proterozoic atmospheric  $p\text{O}_2$  (<0.1–1% PAL) suggested recently by Cr isotope measurements (Fig. 6; Cole et al., 2016; Crowe et al., 2013; Planavsky et al., 2014). Collectively, the two proxies may provide evidence for a disequilibrium between the atmosphere and surface ocean favored by *in situ* photosynthetic oxygen production in the shallow waters (Reinhard et al., 2016). Alternatively, the apparent discrepancy could reflect the uncertainties in our current understanding of modern iodine (Chance et al., 2014; Luther III et al., 1995) and chromium cycling (compare Gilleaudeau et al., 2016 and Planavsky et al., 2014).

$\text{I}/(\text{Ca}+\text{Mg})$  ratios also provide new constraints on the degree of mixing of near-surface oxic waters with shallow anoxic waters (Lu et al., 2016). Given the consistently low maximum  $\text{I}/(\text{Ca}+\text{Mg})$  ratios observed through most of the Proterozoic relative to the Phanerozoic (Fig. 6), we suggest that the iodine record most strongly supports a weakly oxidized surface ocean with shallow anoxic waters near or within the surface ocean for most of the Proterozoic. In other words, Proterozoic surface ocean redox was analogous to the oxycline of modern anoxic basins and OMZs (Fig. 1). These modern settings—where oxygen is locally present, but  $\text{IO}_3^-$  reduction is active in resident and/or adjacent exchanging water masses—are characterized by sustained  $\text{IO}_3^-$  accumulation, but with diagnostically low concentrations and correspondingly low  $\text{I}/(\text{Ca}+\text{Mg})$  ratios in the range observed throughout the Proterozoic (yellow squares, Fig. 6). That pattern manifests in a predominance of low  $\text{I}/(\text{Ca}+\text{Mg})$  ratios during the Proterozoic interrupted only episodically by largely minor increases (Fig. 6) during some intervals previously described as oxygenation events. These include the GOE (Lyons et al., 2014), the Lomagundi excursion (Fig. 6; Bekker and Holland, 2012), at 1.4 Ga (Mukherjee and Large, 2016), the Neoproterozoic broadly (Planavsky et al., 2014), and the Shuram anomaly (Fike et al., 2006). Collectively, these trends suggest a history of protracted and dynamic oxygenation within a largely anoxic ocean (Reinhard et al., 2013; Sperling et al., 2015) through the Proterozoic—rather than a unidirectional rise.

We specifically link the generally low but non-zero mid-Proterozoic iodine values to an extremely shallow oxycline that

facilitated direct advective exchange between weakly oxic surface waters and underlying or adjacent waters that were dominantly anoxic (Reinhard et al., 2013; Sperling et al., 2015). Reinforcing this interpretation, mid-Proterozoic records of chromium isotopes (Planavsky et al., 2014), Mo and Cr concentrations (Reinhard et al., 2013), U concentrations (Partin et al., 2013), rare earth elements (Tang et al., 2016), Zn/Fe ratios (Liu et al., 2016), and CAS (e.g., Kah et al., 2004) all indicate limited mid-Proterozoic biospheric oxygenation. Independent evidence for the restriction of mid-Proterozoic marine oxygen to shallow near-shore settings comes from nitrogen isotopes from multiple mid-Proterozoic proximal to distal facies transects, which indicate an onshore–offshore gradient in the extent of aerobic nitrogen cycling, and thus nitrate availability (Koehler et al., 2017)—an anion with a similar redox sensitivity to that of  $\text{IO}_3^-$  (Emerson et al., 1979; Farrenkopf and Luther III, 2002; Kennedy and Elderfield, 1987a, 1987b; Rue et al., 1997; Wong and Brewer, 1977). In such a setting, it is likely that both upward and lateral mixing of  $\text{O}_2$ -free waters frequently perturbed and intruded into already poorly oxygenated shallow ocean waters. Together with independent evidence for mid-depth euxinia throughout the mid-Proterozoic based on iron speciation analysis of shale (Fig. 6), the upward and lateral mixing of anoxic waters into weakly oxygenated surface waters may also have resulted in frequent episodic incursions of hydrogen sulfide into particularly shallow settings.

## 6. Summary and implications for Proterozoic life

The Proterozoic iodine record provides a comprehensive window to oxygen dynamics that may have dominated ancient, marginal shallow-marine settings—the ecological hot spots that likely hosted the emergence and diversification of eukaryotes, including animals (Jablonski et al., 1983; Knoll, 2014). This distinction highlights the value of  $I/(\text{Ca}+\text{Mg})$  data relative to other Proterozoic paleoredox records that are specific to atmospheric (Cr isotopes) or deep-marine anoxia (trace metals and Fe mineral speciation in shales). The overarching trends in our dataset are not easily linked to diagenetic processes, and there is strong support for a primary origin of iodine records across the heavily discussed Shuram excursion.

Previous debate regarding the potential for redox controls on the timing of early animal evolution has focused on experimental and ecological analyses of animal physiology (Mills et al., 2014; Sperling et al., 2013) as related to indirect estimates of atmospheric  $p\text{O}_2$  (Planavsky et al., 2014). The iodine data provide a more direct perspective, suggesting the possibility of a Proterozoic surface ocean that was at least intermittently hospitable to eukaryotes and that may have been at, near, or above the lower limits of oxygen required for small, simple (but not large and energetic) animals (Mills et al., 2014; Sperling et al., 2013). Critically, however, our data also support the likelihood that the marginal shelf settings in which early protistan and, later, animal fossils are found were characterized by low and variable  $\text{O}_2$  conditions (Gilleaudeau and Kah, 2015; Reinhard et al., 2016) most analogous to those within the oxycline directly overlying modern OMZs and within anoxic basins. We argue that these conditions were particularly common through the mid-Proterozoic, with weakly oxygenated shallow waters impacted frequently if not persistently by upward and lateral intrusion of abundant anoxic waters. Despite maximum shallow ocean  $[\text{O}_2]$  that was likely near the proposed thresholds for simple, early animals, such dynamic conditions could have challenged eukaryotic and, later, animal emergence and diversification during the mid-Proterozoic for at least a billion years (Johnston et al., 2012).

## Author contributions

DH, ZL, XZ and CD analyzed  $I/(\text{Ca}+\text{Mg})$  ratios. AB, BG, CW, DH, GJ, LK, AK, SL, MO, NP and PS provided sample material or aided with fieldwork. DH designed the study and wrote the manuscript, with major contributions from ZL and TL. MO, NP and AB also provided essential input throughout. All authors discussed the results and commented on and approved manuscript submission.

## Acknowledgements

TL, ZL, and DH thank NSF EAR-1349252. ZL further thanks OCE-1232620. DH, ZL, and TL acknowledge further funding from a NASA Early Career Collaboration Award. TL, AB, NP, DH, and AK thank the NASA Astrobiology Institute (under Cooperative Agreement No. NNA15BB03A issued through the Science Mission Directorate). TL and NP received support from the Earth-Life Transitions Program of the National Science Foundation (under Award No. EAR-1338299). AB acknowledges support from NSF grant EAR-05-45484 and an NSERC Discovery and Accelerator Grants. CW acknowledges support from NSF grant 40972021. We also thank Peter Swart for providing the Unda and Clino drill cores, which was supported by NSF funding (OCE-8917295) to PS. We also thank Masha Prokopenko for contribution of carbon isotope values from some GBB short cores. The authors also thank two reviewers for insightful comments that greatly improved this work.

## Appendix A. Supplementary material

Supplementary material related to this article can be found online at <http://dx.doi.org/10.1016/j.epsl.2017.01.032>.

## References

- Bekker, A., Holland, H., 2012. Oxygen overshoot and recovery during the early Paleoproterozoic. *Earth Planet. Sci. Lett.* 317, 295–304.
- Blättler, C.L., Miller, N.R., Higgins, J.A., 2015. Mg and Ca isotope signatures of authigenic dolomite in siliceous deep-sea sediments. *Earth Planet. Sci. Lett.* 419, 32–42.
- Bristow, T.F., Kennedy, M.J., 2008. Carbon isotope excursions and the oxidant budget of the Ediacaran atmosphere and ocean. *Geology* 36, 863–866.
- Brocks, J., Jarrett, A., Sirantoine, E., Kenig, F., Moczyłowska, M., Porter, S., Hope, J., 2016. Early sponges and toxic protists: possible sources of cryostane, an age diagnostic biomarker antedating Sturtian Snowball Earth. *Geobiology* 14, 129–149.
- Chance, R., Baker, A.R., Carpenter, L., Jickells, T.D., 2014. The distribution of iodide at the sea surface. *Environ. Sci., Process. Impacts* 16, 1841–1859.
- Cole, D.B., Reinhard, C.T., Wang, X., Gueguen, B., Halverson, G.P., Gibson, T., Hodgskiss, M.S., McKenzie, N.R., Lyons, T.W., Planavsky, N.J., 2016. A shale-hosted Cr isotope record of low atmospheric oxygen during the Proterozoic. *Geology* 44, 555–558.
- Crowe, S.A., Døssing, L.N., Beukes, N.J., Bau, M., Kruger, S.J., Frei, R., Canfield, D.E., 2013. Atmospheric oxygenation three billion years ago. *Nature* 501, 535–538.
- Derry, L.A., 2010. A burial diagenesis origin for the Ediacaran Shuram–Wonoka carbon isotope anomaly. *Earth Planet. Sci. Lett.* 294, 152–162.
- Emerson, S., Cranston, R.E., Liss, P.S., 1979. Redox species in a reducing fjord: equilibrium and kinetic considerations. *Deep-Sea Res., A, Oceanogr. Res. Pap.* 26, 859–878.
- Fairchild, I.J., Knoll, A.H., Swett, K., 1991. Coastal lithofacies and biofacies associated with syndepositional dolomitization and silicification (Draken Formation, Upper Riphean, Svalbard). *Precambrian Res.* 53, 165–197.
- Farrenkopf, A.M., Dollhopf, M.E., Chadhain, S.N., Luther III, G.W., Nealson, K.H., 1997. Reduction of iodate in seawater during Arabian Sea shipboard incubations and in laboratory cultures of the marine bacterium *Shewanella putrefaciens* strain MR-4. *Mar. Chem.* 57, 347–354.
- Farrenkopf, A.M., Luther III, G.W., 2002. Iodine chemistry reflects productivity and denitrification in the Arabian Sea: evidence for flux of dissolved species from sediments of western India into the OMZ. *Deep-Sea Res., Part 2: Top. Stud. Oceanogr.* 49, 2303–2318.
- Fehn, U., 2012. Tracing crustal fluids: applications of natural  $^{129}\text{I}$  and  $^{36}\text{Cl}$ . *Annu. Rev. Earth Planet. Sci.* 40, 45.
- Fike, D.A., Grotzinger, J.P., Pratt, L.M., Summons, R.E., 2006. Oxidation of the Ediacaran ocean. *Nature* 444, 744–747.
- Gill, B.C., Lyons, T.W., Frank, T.D., 2008. Behavior of carbonate-associated sulfate during meteoric diagenesis and implications for the sulfur isotope paleoproxy. *Geochim. Cosmochim. Acta* 72, 4699–4711.

- Gilleaudeau, G., Frei, R., Kaufman, A., Kah, L., Azmy, K., Bartley, J., Chernyavskiy, P., Knoll, A., 2016. Oxygenation of the mid-Proterozoic atmosphere: clues from chromium isotopes in carbonates. *Geochim. Perspect. Lett.* 2, 178–187.
- Gilleaudeau, G.J., Kah, L.C., 2015. Heterogeneous redox conditions and a shallow chemocline in the Mesoproterozoic ocean: evidence from carbon–sulfur–iron relationships. *Precambrian Res.* 257, 94–108.
- Glock, N., Liebetrau, V., Eisenhauer, A., 2014. I/Ca ratios in benthic foraminifera from the Peruvian oxygen minimum zone: analytical methodology and evaluation as proxy for redox conditions. *Biogeosci. Discuss.* 11, 11635–11670.
- Hardisty, D.S., Lu, Z., Planavsky, N.J., Bekker, A., Philippot, P., Zhou, X., Lyons, T.W., 2014. An iodine record of Paleoproterozoic surface ocean oxygenation. *Geology* 42, 619–622.
- Husson, J.M., Higgins, J.A., Maloof, A.C., Schoene, B., 2015. Ca and Mg isotope constraints on the origin of Earth's deepest  $\delta^{13}\text{C}$  excursion. *Geochim. Cosmochim. Acta* 160, 243–266.
- Jablonski, D., Sepkoski, J.J., Bottjer, D.J., Sheehan, P.M., 1983. Onshore–offshore patterns in the evolution of Phanerozoic shelf communities. *Science* 222, 1123–1125.
- Johnston, D., Poulton, S., Goldberg, T., Sergeev, V., Podkovyrov, V., Vorob'eva, N., Bekker, A., Knoll, A., 2012. Late Ediacaran redox stability and metazoan evolution. *Earth Planet. Sci. Lett.* 335, 25–35.
- Johnston, D.T., Poulton, S., Tosca, N., O'Brien, T., Halverson, G., Schrag, D., Macdonald, F., 2013. Searching for an oxygenation event in the fossiliferous Ediacaran of northwestern Canada. *Chem. Geol.* 362, 273–286.
- Kah, L.C., 2000. Depositional  $\delta^{18}\text{O}$  signatures in Proterozoic dolostones: constraints on seawater chemistry and early diagenesis. *SEPM Spec. Publ.* 67.
- Kah, L.C., Lyons, T.W., Frank, T.D., 2004. Low marine sulphate and protracted oxygenation of the Proterozoic biosphere. *Nature* 431, 834–838.
- Kaufman, A.J., Corsetti, F.A., Varni, M.A., 2007. The effect of rising atmospheric oxygen on carbon and sulfur isotope anomalies in the Neoproterozoic Johnnie Formation, Death Valley, USA. *Chem. Geol.* 237, 47–63.
- Kennedy, H., Elderfield, H., 1987a. Iodine diagenesis in non-pelagic deep-sea sediments. *Geochim. Cosmochim. Acta* 51, 2505–2514.
- Kennedy, H.A., Elderfield, H., 1987b. Iodine diagenesis in pelagic deep-sea sediments. *Geochim. Cosmochim. Acta* 51, 2489–2504.
- Kenter, J.A., Ginsburg, R.N., Troelstra, S.R., 2001. Sea-level-driven sedimentation patterns on the slope and margin. *SEPM Spec. Publ.* 70, 61–100.
- Knoll, A.H., 2014. Paleobiological perspectives on early eukaryotic evolution. *Cold Spring Harb. Perspect. Biol.* 6, a016121.
- Koehler, M.C., Stüeken, E.E., Kipp, M.A., Buick, R., Knoll, A.H., 2017. Spatial and temporal trends in Precambrian nitrogen cycling: a Mesoproterozoic offshore nitrate minimum. *Geochim. Cosmochim. Acta* 198, 315–337.
- Lee, C., Love, G.D., Fischer, W.W., Grotzinger, J.P., Halverson, G.P., 2015. Marine organic matter cycling during the Ediacaran Shuram excursion. *Geology* 43, 1103–1106.
- Liu, X., Kah, L., Knoll, A., Cui, H., Kaufman, A., Shahar, A., Hazen, R., 2016. Tracing Earth's  $\text{O}_2$  evolution using Zn/Fe ratios in marine carbonates. *Geochim. Perspect. Lett.* 2, 24–34.
- Loope, G.R., Kump, L.R., Arthur, M.A., 2013. Shallow water redox conditions from the Permian–Triassic boundary microbialite: the rare earth element and iodine geochemistry of carbonates from Turkey and South China. *Chem. Geol.* 351, 195–208.
- Loyd, S.J., Berelson, W.M., Lyons, T.W., Hammond, D.E., Corsetti, F.A., 2012. Constraining pathways of microbial mediation for carbonate concretions of the Miocene Monterey Formation using carbonate-associated sulfate. *Geochim. Cosmochim. Acta* 78, 77–98.
- Loyd, S.J., Marengo, P.J., Hagadorn, J.W., Lyons, T.W., Kaufman, A.J., Sour-Tovar, F., Corsetti, F.A., 2013. Local  $\delta^{34}\text{S}$  variability in 580 Ma carbonates of northwestern Mexico and the Neoproterozoic marine sulfate reservoir. *Precambrian Res.* 224, 551–569.
- Lu, Z., Hoogakker, B.A., Hillenbrand, C.-D., Zhou, X., Thomas, E., Gutchess, K.M., Lu, W., Jones, L., Rickaby, R.E., 2016. Oxygen depletion recorded in upper waters of the glacial Southern Ocean. *Nat. Commun.* 7.
- Lu, Z., Jenkyns, H.C., Rickaby, R.E., 2010. Iodine to calcium ratios in marine carbonate as a paleo-redox proxy during oceanic anoxic events. *Geology* 38, 1107–1110.
- Luther III, G.W., Wu, J., Cullen, J.B., 1995. Redox chemistry of iodine in seawater: frontier molecular orbital theory considerations. In: *Aquatic Chemistry: Interfacial and Interspecies Processes*, vol. 244. p. 135.
- Lyons, T.W., Reinhard, C.T., Planavsky, N.J., 2014. The rise of oxygen in Earth's early ocean and atmosphere. *Nature* 506, 307–315.
- Manfrino, C.M., Ginsburg, R.N., 2001. Pliocene to Pleistocene deposition history of the upper platform margin. *SEPM Spec. Publ.* 70, 17–39.
- McClain, M.E., Swart, P.K., Vacher, H.L., 1992. The hydrogeochemistry of early meteoric diagenesis in a Holocene deposit of biogenic carbonates. *J. Sediment. Res.* 62.
- Melim, L.A., Swart, P.K., Maliva, R.G., 1995. Meteoric-like fabrics forming in marine waters: implications for the use of petrography to identify diagenetic environments. *Geology* 23, 755–758.
- Mills, D.B., Ward, L.M., Jones, C., Sweeten, B., Forth, M., Treusch, A.H., Canfield, D.E., 2014. Oxygen requirements of the earliest animals. *Proc. Natl. Acad. Sci.* 111, 4168–4172.
- Mitchell, R., Sheldon, N., 2009. Weathering and paleosol formation in the 1.1 Ga Keweenaw Rift. *Precambrian Res.* 168, 271–283.
- Mukherjee, I., Large, R.R., 2016. Pyrite trace element chemistry of the Velkerri formation, Roper group, McArthur basin: evidence for atmospheric oxygenation during the boring billion. *Precambrian Res.* 28, 13–26.
- Muramatsu, Y., Wedepohl, K., Hans, 1998. The distribution of iodine in the Earth's crust. *Chem. Geol.* 147, 201–216.
- Osburn, M.R., Owens, J., Bergmann, K.D., Lyons, T.W., Grotzinger, J.P., 2015. Dynamic changes in sulfate sulfur isotopes preceding the Ediacaran Shuram Excursion. *Geochim. Cosmochim. Acta* 170, 204–224.
- Owens, J.D., Lyons, T.W., Hardisty, D.S., Lowery, C.M., Lu, Z., Lee, B., Jenkyns, H.C., 2017. Patterns of local and global redox variability during the Cenomanian–Turonian Boundary Event (Oceanic Anoxic Event 2) recorded in carbonates and shales from central Italy. *Sedimentology* 64, 168–185.
- Partin, C., Bekker, A., Planavsky, N., Scott, C., Gill, B., Li, C., Podkovyrov, V., Maslov, A., Konhauser, K., Lalonde, S., 2013. Large-scale fluctuations in Precambrian atmospheric and oceanic oxygen levels from the record of U in shales. *Earth Planet. Sci. Lett.* 369, 284–293.
- Pisarevsky, S.A., Murphy, J.B., Cawood, P.A., Collins, A.S., 2008. Late Neoproterozoic and Early Cambrian Palaeogeography: Models and Problems. *Spec. Publ.*, vol. 294. Geological Society, London, pp. 9–31.
- Planavsky, N.J., Reinhard, C.T., Wang, X., Thomson, D., McGoldrick, P., Rainbird, R.H., Johnson, T., Fischer, W.W., Lyons, T.W., 2014. Low Mid-Proterozoic atmospheric oxygen levels and the delayed rise of animals. *Science* 346, 635–638.
- Reinhard, C.T., Planavsky, N.J., Olson, S.L., Lyons, T.W., Erwin, D.H., 2016. Earth's oxygen cycle and the evolution of animal life. *Proc. Natl. Acad. Sci.* 113, 8933–8938.
- Reinhard, C.T., Planavsky, N.J., Robbins, L.J., Partin, C.A., Gill, B.C., Lalonde, S.V., Bekker, A., Konhauser, K.O., Lyons, T.W., 2013. Proterozoic ocean redox and biogeochemical stasis. *Proc. Natl. Acad. Sci.* 110, 5357–5362.
- Romaniello, S.J., Herrmann, A.D., Anbar, A.D., 2013. Uranium concentrations and  $^{238}\text{U}/^{235}\text{U}$  isotope ratios in modern carbonates from the Bahamas: assessing a novel paleoredox proxy. *Chem. Geol.* 362, 305–316.
- Rothman, D.H., Hayes, J.M., Summons, R.E., 2003. Dynamics of the Neoproterozoic carbon cycle. *Proc. Natl. Acad. Sci.* 100, 8124–8129.
- Rue, E.L., Smith, G.J., Cutter, G.A., Bruland, K.W., 1997. The response of trace element redox couples to suboxic conditions in the water column. *Deep-Sea Res., Part 1: Oceanogr. Res. Pap.* 44, 113–134.
- Schrag, D.P., Higgins, J.A., Macdonald, F.A., Johnston, D.T., 2013. Authigenic carbonate and the history of the global carbon cycle. *Science* 339, 540–543.
- Sperling, E.A., Halverson, G.P., Knoll, A.H., Macdonald, F.A., Johnston, D.T., 2013. A basin redox transect at the dawn of animal life. *Earth Planet. Sci. Lett.* 371, 143–155.
- Sperling, E.A., Wolock, C.J., Morgan, A.S., Gill, B.C., Kunzmann, M., Halverson, G.P., Macdonald, F.A., Knoll, A.H., Johnston, D.T., 2015. Statistical analysis of iron geochemical data suggests limited late Proterozoic oxygenation. *Nature* 523, 451–454.
- Swart, P.K., Kennedy, M.J., 2012. Does the global stratigraphic reproducibility of  $\delta^{13}\text{C}$  in Neoproterozoic carbonates require a marine origin? A Pliocene–Pleistocene comparison. *Geology* 40, 87–90.
- Swart, P.K., Melim, L.A., 2000. The origin of dolomites in Tertiary sediments from the margin of Great Bahama Bank. *J. Sediment. Res.* 70, 738–748.
- Tang, D., Shi, X., Wang, X., Jiang, G., 2016. Extremely low oxygen concentration in mid-Proterozoic shallow seawaters. *Precambrian Res.* 276, 145–157.
- Tucker, M.E., 1982. Precambrian dolomites: petrographic and isotopic evidence that they differ from Phanerozoic dolomites. *Geology* 10, 7–12.
- Vahrenkamp, V., Swart, P., 1994. Late Cenozoic dolomites of the Bahamas: metastable analogues for the genesis of ancient platform dolomites. In: *Dolomites: A Volume in Honour of Dolomieu*, vol. 21, pp. 133–153.
- van Smeerdijk Hood, A., Wallace, M.W., Drysdale, R.N., 2011. Neoproterozoic aragonite–dolomite seas? Widespread marine dolomite precipitation in Cryogenian reef complexes. *Geology* 39, 871–874.
- Wong, G.T., Brewer, P.G., 1977. The marine chemistry of iodine in anoxic basins. *Geochim. Cosmochim. Acta* 41, 151–159.
- Zhang, S., Henehan, M.J., Hull, P.M., Reid, R.P., Hardisty, D.S., Hood, A., Planavsky, N.J., 2017. Environmental and biological controls on boron isotope ratios in shallow marine carbonates. *Earth Planet. Sci. Lett.* 458, 380–393.
- Zhao, M.-Y., Zheng, Y.-F., Zhao, Y.-Y., 2016. Seeking a geochemical identifier for authigenic carbonate. *Nat. Commun.* 7.
- Zhou, X., Jenkyns, H.C., Owens, J.D., Junium, C.K., Zheng, X.Y., Sageman, B.B., Hardisty, D.S., Lyons, T.W., Ridgwell, A., Lu, Z., 2015. Upper ocean oxygenation dynamics from I/Ca ratios during the Cenomanian–Turonian OAE 2. *Paleoceanography* 30 (5), 510–526.
- Zhou, X., Thomas, E., Rickaby, R.E., Winguth, A.M., Lu, Z., 2014. I/Ca evidence for upper ocean deoxygenation during the PETM. *Paleoceanography* 29, 964–975.